Quantitative Particle-Induced X-ray Emission Imaging of Rat Olfactory Epithelium Applied to the Permeability of Rat Epithelium to Inhaled Aluminum

Kevin K. Divine,[†] Johnnye L. Lewis,[‡] Patrick G. Grant,[§] and Graham Bench*,[§]

*Lovelace Respiratory Research Institute, P.O. Box 5890, Albuquerque, New Mexico 87185,
Center for Population Health, University of New Mexico, Albuquerque, New Mexico 87131-5267, and
Center for Accelerator Mass Spectrometry, Lawrence Livermore National Laboratory,
Livermore, California 94550*

Neurotoxicity from chronic metal inhalation has been suggested as an underlying contributor to late-developing neurodegenerative diseases that have symptoms similar to Alzheimer's and Parkinson's syndromes. If inhaled metals contribute to pathogenesis of these diseases, identifying, localizing, and quantitating metal deposition(s) within specific target regions of the central nervous system will be critical to our understanding of the mechanisms. Standard analytical techniques used to date require exposure to extremely high concentrations of metals to meet analytical detection limits in small tissue areas. The relevance to lower-dose environmentally relevant exposures and potential protective barriers is therefore questionable. The feasibility of microbeam particle-induced X-ray emission is investigated as a method for rapidly scanning tissues to study the inhalation of metals, nasal permeability, and central nervous system deposition. The optimal beam spot and analysis time used to image the rat olfactory epithelium to facilitate the rapid detection of aluminum localizations were determined. Measurements of aluminum localizations in rat olfactory bulb and brain sections are also presented.

Introduction

Chronic metal inhalation is thought to be involved in the neurotoxicology of neurodegenerative diseases that have symptoms similar to Alzheimer's and Parkinson's syndromes (*1*). This relationship has been hypothesized using epidemiological data from occupational exposure to metal dust(s) (Al, Cd, and Mn) found in mining operations and/or other occupational exposures (*2–4*). In a recent study of Parkinson's disease in twins, it was determined that a majority of cases were not genetically caused but were by implication environmentally caused (*5*). In addition, Al has been linked with Alzheimer's disease due in large part to its often-cited presence in the cores of neuritic plaques of Alzheimer's patients. Initially, dietary intake of Al was thought to be the route of exposure, however, because Al is poorly absorbed from the gastrointestinal tract, this theory has met with controversy and skepticism. Alternative proposals have focused on inhalation of Al as a possible route of exposure. Olfactory neurons are in contact with both the nasal lumen and the olfactory bulbs, making them nearly the first tissue accessible to inhaled toxicants and potentially providing a direct single-cell pathway to the central nervous system (CNS).[1] Previous investigators have demonstrated that several materials, including metals, have the ability to translocate to the olfactory bulb following nasal instillation (*6–9*). The environmental relevance of these studies is difficult to determine because (1) the exposures were conducted via instillation or an invasive surgical technique, (2) the histopathology of the olfactory mucosa confirming no damage from the instillation or surgical technique often was not present, and (3) large doses of materials were used. Conducting experiments designed to determine if Al and/or other metals translocate to the olfactory bulb following inhalation of environmentally relevant concentrations requires an analytical technique that combines accurate quantitation, low detection limits, and a high degree of spatial resolution.

Many different methods have been applied in mapping the spatial distribution of elemental constituents in tissues (*10*). However, none combine the ability to conduct several simultaneous quantitative measurements at parts per million sensitivity and fine spatial resolution and with a minimal effect upon the specimen. For instance, fluorescent dye or monoclonal antibody staining techniques coupled with light and electron microscopy provide only limited quantitation and require specific antibodies that often are not available for all free metals. Electron microprobe X-ray analysis utilizing energy-dispersive X-ray detectors can produce sub-micrometer beam spots, but detection sensitivities are in the range of several hundred to a few thousand parts per million

---

* To whom correspondence should be addressed: CAMS, L-397, Lawrence Livermore National Laboratory, Livermore, CA 94550. Phone: (925) 423-5155. Fax: (925) 423-7884. E-mail: bench1@llnl.gov.
† Lovelace Respiratory Research Institute.
‡ University of New Mexico.
§ Lawrence Livermore National Laboratory.

[1] Abbreviations: CNS, central nervous system; SIMS, secondary ion mass spectrometry; ICP-MS, inductively coupled plasma mass spectrometry; μ-PIXE, microbeam particle-induced X-ray emission; STIM, scanning transmission ion microscopy; IMAP, Ion Micro Analysis Package; PIXEF, particle-induced X-ray emission spectrum fitting code; mdl, minimum detection limit.

(*11*). X-ray fluorescence has element-detection sensitivities in the parts per million range, but the spatial resolution is typically limited to ≥10 μm. In the imaging mode, secondary ion mass spectrometry (SIMS) usually has a spatial resolution of ~1 μm and parts per million to parts per billion sensitivity. However, in general SIMS can be difficult to perform quantitatively (*11*). Like SIMS, elemental quantitation using laser microprobe mass analysis is often difficult, although spatial resolution is in the 1 μm range (*11*). Last, inductively coupled plasma mass spectrometry (ICP-MS) has detection limits that range from parts per billion to part per trillion; however, ICP-MS relies on homogenization, and as such, the spatial resolution is limited to the size of the area used to prepare the sample. In addition, although a sample may contain discrete areas with metal concentrations above the detection limit, homogenization can dilute the overall metal concentration to below the detection limit through the inclusion of regions containing no metal.

Nuclear microscopy (*12*), specifically with Microbeam PIXE (μ-PIXE) (*13*), has previously been used to study metal content at the cellular level in various cells and tissue types and potentially is ideally suited for investigating inhaled metal contaminants. μ-PIXE uses a rastered megaelectronvolt energy proton beam to provide the micrometer scale spatial resolution required for analyzing brain nuclei while still maintaining simultaneous parts per million (w/w) multielement detection. The penetration depth of megaelectronvolt protons (~100 μm in biological material for 3 MeV protons) allows μ-PIXE to measure the total elemental contents within cells or tissue sections that are several micrometers thick. The parts per million detection limit may make it possible to collect meaningful data from animals exposed to environmentally relevant metal concentrations. In addition, simultaneous quantitation and localization of numerous metals may be advantageous since it is hypothesized that multiple metals may utilize the same transport mechanism. Another potential advantage is that using only one method to quantitate metal concentration(s) and provide spatial information reduces the probability of introducing contaminants that can alter concentrations and/or localizations. However, a significant drawback in the use of μ-PIXE is the relatively long analysis time required for examining large specimens at fine spatial resolution. μ-PIXE data acquisition times are determined by the number of X-rays that are detected per unit time interval. The rat olfactory bulb is approximately 4 mm × 4 mm. At present, to identify one metal localization in a 4 mm × 4 mm area at a spatial resolution of 1 μm requires 1 day of accelerator time. Obviously, this analysis time is too long, too costly, and prohibitively expensive for routine analysis of biological samples. Therefore, to increase the utility of μ-PIXE for analyzing large tissue sections, methods must be developed that significantly decrease analysis times while not degrading detection limits and/or spatial localization.

The objective of this study is to test the hypothesis that rapid, large-area, low-resolution scans using broad beam (10−50 μm) μ-PIXE can be employed to identify areas of metal localization. Fine beam (1−10 μm) μ-PIXE scans could then be used to provide fine spatial resolution only within regions identified to have metal localizations. This will require determining an optimal beam size for the broad beam μ-PIXE scans, one where narrowing the beam will not significantly enhance sensitivity although

it may significantly enhance localization. If successful, the μ-PIXE technique will be a useful and relatively inexpensive way to examine metal uptake and distribution in biological samples. Al is at the low end of the X-ray dynamic range of many PIXE X-ray detector systems and has a relatively high minimum detection limit. Thus, demonstration and validation of these methods using tissues obtained from Al-exposed animals will provide strong support for the utility of this technique in assessing a broad range of elemental analyses of interest in physiological systems.

Materials and Methods

All experiments reported here were approved by both the Lawrence Livermore National Laboratory and Lovelace Respiratory Research Institute animal care and use committees.

Chemicals. Aluminum chlorohydrate was the source of inhaled Al (Pfaltz & Bauer, Waterbury, CT). The thin film Al standard of thickness (50.8 μg/cm^2) used to calibrate the X-ray detection efficiency for Al was obtained from Micromatter (Seattle, WA).

Animal Exposures. Fisher 344 (Harlan Sprague-Dawley, Indianapolis, IN) rats were exposed to Al (20.60 ± 1.96 μg/m^3) via nose-only exposure. Exposures were for 6 hours/day for 12 days. The animals were sacrificed 30 min following the final exposure. To ensure that the schedule was adhered to, start times were staggered. The exposure apparatus was a multiport chamber designed specifically for small animal exposure (*14*). The flow rate was 20 L/min. Aerosols were generated by a venturi powder disperser (*15*). Confirmation of exposure atmospheres was carried out by measuring the flow rate, aerosol concentration, and size distribution of the particles. The flow rate was measured by rotameters. Aerosol characterization used samples collected on Zefluor filters (1 μm pore size, 25 mm diameter, Gelman Sciences, Ann Arbor, MI). The aerosol concentration was calculated by dividing the mass of particles collected on the Zefluor filters by the total amount of air flow during the collection period. The particle size distribution was determined using a Lovelace multijet cascade impactor (In-Tox Products, Albuquerque, NM) three times during each exposure. The concentration was also monitored continuously with a light scattering mass monitor (RAM-S monitor, GCA, Bedford, CT). We have also performed similar nose-only exposure experiments on rats not involving exposure to aluminum. Brain tissue sections were prepared using the same sample preparation and PIXE analysis protocols reported here. Analysis of brain tissue sections from these non-aluminum nose-only exposures has not revealed any aluminum localizations down to the limits of detection for the PIXE measurements. Consequently, as we are concentrating on analytical methodology in this paper, we will focus solely on the aluminum inhalation exposures.

Tissue Sample Preparation. Obsidian knives, nylon, and Teflon-coated instruments were used to avoid contaminating the tissue samples during processing. In addition, all reagents that were used in these experiments were of a grade ensured to be free of trace metals. The rats were anesthetized by carbon dioxide inhalation and exsanguinated by cardiac puncture and intracardial saline perfusion. Following perfusion, the dorsal surface of the skull was removed to the cribform plate, the dura cut and retracted from the brain, and the olfactory nerve severed, and the brain and olfactory bulbs were removed. To ensure no leaching of deposited metals, the tissue was frozen rather than fixed. The brains of the animals were sectioned down the midline, and each half was separately frozen in isopentane cooled with liquid nitrogen. The brains were then cryosectioned into 10 μm sagittal sections. Sections were bisected into anterior and posterior halves. The sections were mounted on precooled nylon foils, freeze-dried, and stored in a sterile environment until μ-PIXE analysis.

Nuclear Microscopy. Samples were examined at the nuclear microprobe facility at the Lawrence Livermore National Labora-

tory. The nuclear microprobe can focus a 100 pA, 3 MeV energy proton beam with beam spot diameters of <1 μm (*16*). The 25 keV H$^-$ ions are produced by an off-axis duoplasmatron ion source and accelerated and stripped in a tandem electrostatic accelerator to produce megaelectronvolt energy protons. These energetic ions subsequently pass through the field of a energy-analyzing magnet and a slit which controls the energy stability of the accelerator. The nuclear microscope lies 0.5 m down-stream of the energy stabilization slit. At the entrance to the proton microscope, the central portion of the beam core is first selected and then further collimated by sets of slits before being focused onto the specimen by a triplet of magnetic quadrupole lenses. The focused beam is scanned over the sample by electrostatic deflection in a point by point raster mode (*17*). The beam dwells at a particular sample location until a preset amount of integrated current or charge has been recorded before stepping onto the next beam location. Samples were analyzed using μ-PIXE to determine element X-ray yields, and scanning transmission ion microscopy (STIM) was used to determine specimen thickness and projected density. Microbeam PIXE causes minimal alteration to the sample (*18*). The megaelectronvolt ion energies cause negligible sputtering of material from the specimen surface and very low radiation damage, while use of <0.2 nA/μm² beam current densities and a scanned beam minimizes thermal damage to biological specimens.

μ-**PIXE Analysis of Tissue Sections.** μ-PIXE utilizes a high-energy (megaelectronvolt) proton beam that interacts primarily with atomic electrons within a specimen to create vacancies in inner shell orbitals. When a vacancy is filled by an outer shell electron, the excess energy resulting from the transition can be released as an X-ray photon whose energy is characteristic of the emitting atom. The lack of primary particle bremsstrahlung enables μ-PIXE to be carried out with little X-ray background compared to the electron analogue producing high analytical sensitivity. Proton-induced X-rays were detected with an energy dispersive Iglet-X X-ray detector (EG&G Ortec, Oakridge, TN) that subtended a solid angle of ~200 msr to the specimen. The detector was located at an angle of 135° with respect to the incident beam. Charge was collected in a Faraday cup located behind the sample. As the beam is scanned across the sample, X-ray energy spectra are stored for each beam location. Within each raster pass, 0.1 nC was deposited to each beam location. After data acquisition, maps of element concentrations were generated from these data and X-ray spectra from beam locations corresponding to any region of interest can be extracted for quantitative analysis (*19*). After being freeze-dried, tissue sections were stored in airtight plastic containers prior to analysis and consequently had minimal exposure (less than 5 min) to laboratory air. Although tissue sections exposed to laboratory air for extended periods of time may acquire Al from dust, brain tissues that we have analyzed via PIXE from animals not exposed to Al have shown no evidence (down to limits of detection) of aluminum localizations. This suggests that, at least in our instance, the possibility that tissue sections obtained sequestered aluminum from airborne dust in the sample preparation and analysis laboratories was slight.

STIM Measurement of Tissue Sections. To normalize μ-PIXE X-ray yields for the projected density of the sample, a measurement of the specimen projected density is required. STIM supplies these data by measuring the energy lost by the incident beam as it traverses the sample. For STIM, residual ion energies were measured with a retractable charged particle silicon surface barrier detector located approximately 5 cm directly behind the sample and in front of the Faraday cup after the beam current had been reduced to ~10000 protons per second by reducing the size of microprobe selection and collimation slits. The surface barrier detector was retracted from the path of the beam during μ-PIXE measurements (the 1 million-fold higher beam currents used for μ-PIXE resulting from the larger slit settings rapidly result in catastrophic detector damage) (*20*). Residual ion energies were recorded in list mode along with coincident beam spatial coordinates arising from scanning the

beam electrostatically over the sample in a point by point raster mode. The residual energy of 19 ions was measured at each beam location. The median value of these 19 residual ion energies was selected to represent the average residual energy of the ion beam at each beam spatial coordinate (*20*).

μ-**PIXE Data Analysis.** PIXE data were stored in a three-dimensional data block (consisting of the *x*-position, *y*-position, and energy) along with the X-ray spectrum produced by the irradiation (parent spectrum) and analyzed off-line with IMAP (Ion Micro-Analysis Package) (*19*). Detected X-ray yields corresponding to a particular energy range were mapped with the selection of an X-ray energy window from the parent spectrum. Energy windows can be chosen so that they incorporate X-ray emission peaks from an element of interest. For instance, the energy window from 1.4 to 1.6 keV was used to display X-rays arising from Al (Al X-ray energies are ~1.5 keV). However, this process does not discriminate between X-rays arising from a particular element emission peak within the window and any continuum background X-rays and X-rays from neighboring X-ray lines that may be present within the energy window. For instance, if the continuum background signal within an energy window is large compared to the size of an element emission peak, the resultant image will be dominated by the background signal, which can mask the distribution of X-rays arising from the element of interest. Therefore, the following correction for background was used.

Analysis of X-ray Spectra. To obtain quantitative elemental concentrations and to generate quantitative elemental maps, the X-ray spectra at each pixel in a data set were analyzed to account for the presence of any continuum X-ray background to extract characteristic X-ray peak areas (or yields) for the elements of interest. Consequently, the computational iterative PIXE spectrum fitting code (PIXEF), in which target matrix effects are calculated in absolute terms for the specimen (*21*), was used to analyze X-ray data (*22*). With this spectrum fitting code, a wide range of tissues may be analyzed with a small suite of appropriately chosen thin film standards used to calibrate the detector efficiency. PIXEF has been tested on a range of certified standards and has a quantitative accuracy of better than 95% for biological samples (*22*).

In addition to calculating the element X-ray yield, PIXEF also determines the minimum number of X-rays needed for the positive identification of a particular element in an X-ray spectrum. This is accomplished by integrating the energy window corresponding to the background signal under the position of the characteristic X-ray peak. The extremes of this energy window are taken to be 3σ from the peak centroid, where σ is the detector energy resolution at the peak centroid. The minimum number of X-rays or minimum detection limit (mdl) was taken to be 3.29 $\times$ $\sqrt{\text{background}}$ (*22*). An element yield that is smaller than the element mdl is not sufficient for positive identification of the element in the X-ray spectrum, and the element concentration is defined to be below the mdl. If the mdl for any given element is greater than the calculated X-ray yield, PIXEF reanalyzes the whole spectrum so that only characteristic X-ray yields are derived for elements that meet minimum detection criteria. Elements whose X-ray yield is calculated to be less than the mdl have their mdls recalculated assuming the element is not present within the analyzed region.

Quantitation of Al. To cross check the detector's X-ray detection efficiency for Al, a thin film Al standard of thickness of 50.8 $\pm$ 2.6 μg/cm² was analyzed under irradiation conditions similar to those used for analysis of the tissue sections. The μ-PIXE analysis yielded a measured Al thickness of 52.1 $\pm$ 1.9 μg/cm² for this standard.

Following μ-PIXE analysis of each tissue section, STIM was used to measure the energy thickness of the irradiated region on each target. STIM measurements revealed that incident 3 MeV protons typically lost ~100 keV in traversing the freeze-dried olfactory bulb and brain sections. The energy thickness measurements were used to correct the Al X-ray yields obtained

from the spectrum fitting code for X-ray attenuation within the samples and for the variation in the rate of X-ray production with ion energy to obtain Al concentrations in milligrams per kilogram of dry weight (*22*). For these corrections, the composition of the biological material was taken to be $C_5H_9O_2N$ (*20*). This assumed specimen composition has an accuracy of a few percent when used to convert energy losses to projected densities in a wide variety of biological matrixes (*20*) as energy losses of megaelectronvolt energy proton beams are quite insensitive to even relatively large changes in biological matrix composition (*20*).

Al concentrations within a pixel or scan area can subsequently be converted to an elemental mass by multiplying the concentration by the tissue projected density (kilograms per square centimeter) obtained from STIM using the approximate sample composition $C_5H_9O_2N$ (*20*) and multiplying the result by the area from which the spectrum was obtained (square centimeters). Note that a knowledge of sample density is not required using this approach. In a similar vein, X-ray minimum detection limits can be converted to a minimum detectable concentration or elemental mass (*20*).

Iterative Rapid-Scan Methodology Validation. A 0.5 mm × 0.5 mm area of a freeze-dried olfactory bulb cryosection from a rat exposed to Al chlorohydrate was initially studied to test the feasibility of μ-PIXE to rapidly scan large areas of freeze-dried sagittal tissue sections to find trace metal localizations for more detailed study. Beam spots of 50 μm × 50 μm, 20 μm × 20 μm, 10 μm × 10 μm, and 5 μm × 5 μm were chosen to rapidly scan the tissue section, while a 1.5 μm × 1.5 μm beam spot size was used to study the irradiated area with fine spatial resolution. For each scan, the pixel size was chosen to correspond to the beam spot size. STIM data were also collected from the same 0.5 mm × 0.5 mm area upon completion of all μ-PIXE data collection. STIM images were recorded using beam spot and pixel sizes of 50 μm × 50 μm, 20 μm × 20 μm, 10 μm × 10 μm, 5 μm × 5 μm, and 1.5 μm × 1.5 μm to enable quantitative element concentrations to be calculated from the μ-PIXE data.

In preliminary studies of olfactory bulb tissue sections, we found that for beam currents above 4 nA, X-ray yields from the tissue sections decreased with irradiation time (indicative of specimen mass loss) for analyses employing 50 μm × 50 μm, 20 μm × 20 μm, 10 μm × 10 μm, and 5 μm × 5 μm beam spot sizes. Further, the larger the beam current, the more rapidly X-ray yields decreased as a function of dose, indicating that the specimen mass loss was probably caused by thermal heating of the specimen. Optical visualization of tissue sections revealed that in some cases the beam caused significant specimen deformation, and in extreme cases, holes could be observed in irradiated tissue areas.

Although beam currents of >10 nA can be obtained for the 50 μm × 50 μm, 20 μm × 20 μm, and 10 μm × 10 μm beam spot sizes, a lower beam current was utilized for the feasibility study to minimize thermal heating and potential damage to the specimens. A beam current of ~2 nA was employed for the 50 μm × 50 μm, 20 μm × 20 μm, 10 μm × 10 μm, and 5 μm × 5 μm beam spot sizes, while a beam current of ~300 pA was employed for the 1.5 μm × 1.5 μm beam spot size (300 pA is close to the maximum current we can obtain in a 1.5 μm × 1.5 μm spot). For these beam currents and spot sizes, X-ray yields of elements per unit dose remained constant throughout irradiation and specimens suffered no discernible morphological changes on the micrometer scale when viewed after irradiation. For each of the four largest beam spot sizes, three irradiations of the selected tissue region were performed in which different charges were deposited to a pixel. Each irradiation deposited a total charge to the sample that was between ~1 to ~20 μC. For each beam spot size, spatial distributions of elements did not change as a function of integrated charge in these multiple measurements, indicating that the element distributions were not affected at the pixel level by these irradiations using beam currents of 2 nA.

Quantitative Localization of Al in Olfactory Bulb and Brain Sections. Sagittal tissue sections through the olfactory bulb and remaining brain from four rats exposed to aluminum chlorohydrate were analyzed for Al content via μ-PIXE. Anterior (containing olfactory bulb) and posterior portions of one tissue section were analyzed per animal. For each tissue, two 1 mm × 1.5 mm regions within the same sagittal section were irradiated with a 10 μm beam spot. One region contained only olfactory bulb tissue, while the other was brain stem nuclei in the region of the substantia nigra which was used to represent nonolfactory tissue. Each image consisted of 100 × 150 pixels so that the pixel size corresponded to the beam spot size of 10 μm × 10 μm. The beam current for these measurements was 2.5 nA, and a dose of 4 nC was deposited to each pixel, yielding a total dose of 60 μC for each irradiation. Each data set took ~6 h to accumulate. Once μ-PIXE data collection was complete, the irradiated area was analyzed via STIM to enable quantitative element concentrations to be calculated from the μ-PIXE data. STIM data were collected with the same 10 μm × 10 μm beam spot and pixel sizes used to collect the μ-PIXE data. No other analyses for the presence of aluminum will be reported here since other analytical techniques have difficulty in providing accurate quantification of trace metals in biological systems on the scale of a few micrometers.

Results

Figure 1 illustrates how PIXEF can be utilized to generate maps of quantitative elemental concentrations by analyzing the X-ray spectra at each pixel in a data set to account for the presence of any continuum X-ray background to extract characteristic X-ray peak areas (or yields) for the elements of interest. Figure 1A shows a map of detected X-ray distribution corresponding to the energy region from 1.4 to 1.6 keV (an energy region that includes the Al K X-ray peak) from a 1 mm × 1 mm area scanned in tissue 4A. The initial location of possible Al localizations is concealed by the background noise. X-ray spectra corresponding to each pixel were then analyzed using PIXEF to generate maps of Al concentration [Figure 1B which only displays pixels in which the number of calculated Al X-rays in a pixel is greater than $3.29\sqrt{B}$ (*B* represents the Al background X-ray yield)]. Figure 1B yields four regions containing detectable amounts of Al within the 1 mm × 1 mm region.

Iterative Rapid-Scan Methodology Validation. The results of the pixel size optimization studies are shown in Table 1 and Figure 2. Beam spot and pixel sizes of 50 μm × 50 μm, 20 μm × 20 μm, 10 μm × 10 μm, 5 μm × 5 μm, and 1.5 μm × 1.5 μm were used in the irradiation of the same 0.5 μm × 0.5 mm area of the olfactory bulb. For each scan, the pixel size was chosen to correspond to the size of the beam spot. As indicated by the data in Table 1, a pixel size of 10 μm × 10 μm was the most efficient in identifying and quantifying the amount of Al within the analyzed region for beam currents of 2−3 nA. The number of Al localizations or Al sites remained constant for beam spot sizes of 10 μm × 10 μm or finer (Table 1), although the number of pixels containing Al increased. No increase in sensitivity or quantitative accuracy was obtained by decreasing the beam spot size to less than 10 μm × 10 μm; however, using finer beam spot sizes did increase the spatial resolution. Figure 2 shows maps of detected X-rays from the energy region from 1.4 to 1.6 keV of the 0.5 mm × 0.5 mm region (1) scanned with a 50 μm beam spot using a 50 μm × 50 μm pixel size and a dose of 100 nC/pixel (Figure 2A) and (2) scanned with a 20 μm beam spot using a 20 μm × 20 μm pixel size and a dose of 16 nC/pixel (Figure 2B). Figure
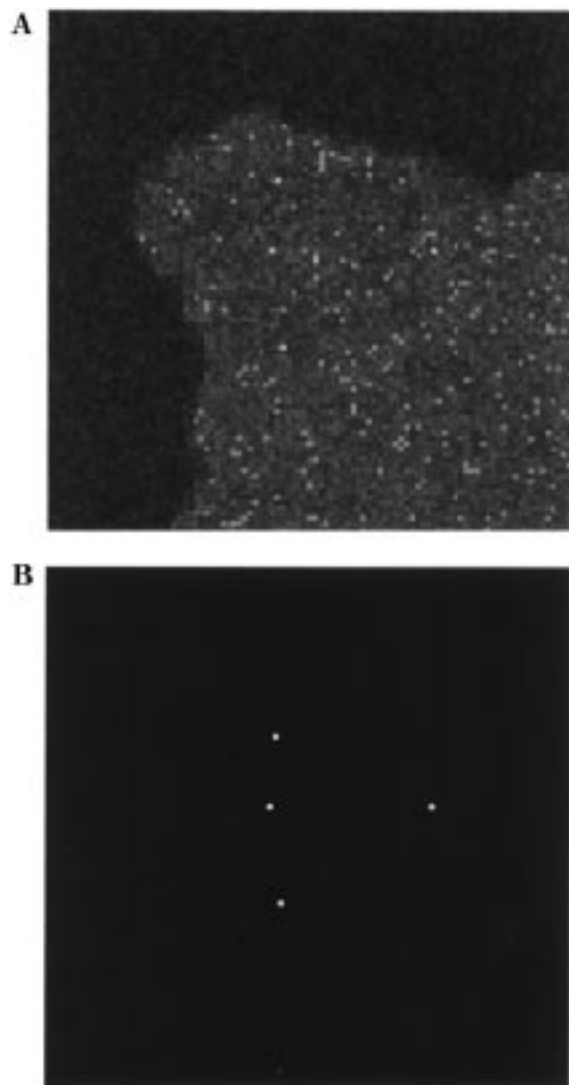
Figure 1. (A) Map of detected X-rays from the energy window from 1.4 to 1.6 keV from a 1 mm × 1 mm region of sample 4a. The image consists of 100 × 100 pixels with a pixel size corresponding to the beam spot size of 10 μm × 10 μm. The beam current used for data collection was 2.5 nA, and a dose of 4 nC was deposited to each pixel, yielding a total dose of 40 μC for the irradiation. It is difficult to discern Al localizations due to the presence of bremmstrahhlung X-rays in the image that produce appreciable noise. (B) Map of the same region shown in panel A displaying those pixels whose Al X-ray yields were greater than or equal to the mdl for Al, i.e., $3.29\sqrt{B}$, where B represents the background X-ray yield associated with the position of the Al peak.

2A reveals only one pixel containing detectable amounts of Al. In comparison with Figure 2A, Figure 2B shows two regions containing detectable amounts of Al, the one previously detected in Figure 2A and an additional pixel.

In Table 1, beam spot and pixel sizes are shown in column 1. Column 2 shows the resulting area of each beam spot associated with the selected beam spot and pixel size. Column 3 displays the approximate analysis time of each irradiation. For each of the 50 μm × 50 μm, 20 μm × 20 μm, 10 μm × 10 μm, and 5 μm × 5 μm beam spot sizes, data were collected for three different accumulated beam charges (column 4). As the charge deposited to each pixel within a given irradiation was constant, column 5 shows the charge (in nanocoulombs) deposited to every pixel in an irradiation and column 6 shows the dose per square micrometer in an irradiation.

Column 7 shows the typical minimum detection limit for Al within a pixel for each irradiation in units of milligrams per kilogram. For each irradiation, this representative minimum detection limit was the average of the minimum detection limits for all pixels containing no detectable Al (as determined by PIXEF) within the scanned region. Column 8 shows the typical minimum detection limit for Al within a pixel for each irradiation in units of picograms. These values were obtained by multiplication of the corresponding value in column 7 by the pixel area and the average projected density of the 0.5 mm × 0.5 mm scanned region determined from the STIM data.

Column 9 shows the number of pixels containing detectable amounts of Al from each irradiation. Column 10 shows the number of pixels in column 8 that register with pixels containing detectable amounts of Al from the irradiation employing the smallest larger pixel size and highest dose per pixel. Column 11 shows the number of detected Al localizations within the scanned region (an Al localization consists of contiguous pixels containing detectable amounts of Al). Column 12 shows the Al mass detected in the scanned region. This mass was obtained by summing the mass of Al from those pixels, which contained detectable amounts of the metal. The mass of Al within each of these pixels was obtained from the concentration of Al in milligrams per kilogram determined by PIXEF multiplied by the area of the pixel and the projected density of the pixel from the registered STIM data. The final column shows the average Al concentration (milligrams per kilogram) detected within the whole 0.5 mm × 0.5 mm scanned region. These values were obtained from the mass of Al detected from each irradiation (column 12) divided by the integrated pixel projected densities within the scanned region and divided by the area covered by one pixel.

Quantitative Localization of Al in Olfactory Bulb and Brain Sections. Table 2 shows results of μ-PIXE analysis of rat olfactory bulbs (1A−4A) and nonolfactory (1B−4B) tissue sections obtained from F344 rats exposed to 20.60 ± 1.96 μg/m³ Al via nose-only exposure for 6 h/day for 12 days. Sample analysis demonstrated that there was a significant difference (as determined by the paired Student's *t* test) between the olfactory bulb and brain tissue both in average Al tissue concentration and number of Al sites observed.

Discussion

The sensitivity of μ-PIXE is dependent on collecting a sufficient number of X-ray emissions from the element of interest over background emissions (primarily bremsstraulung). Increasing the accumulated charge to a specimen improves the counting statistics such that it is easier to identify and quantitate characteristic X-ray peaks. Data from the 50 μm × 50 μm and 20 μm × 20 μm beam spots shown in Table 1 and Figure 2 reveal that using large beam spot sizes results in relatively poor efficiency for identifying micrometer scale localizations and poor accuracy in quantifying the amount of metals within the sample. This poor efficiency is due to the inhomogeneity in Al distribution throughout the sample tissue. Improving the spatial resolution from 50 μm × 50 μm, through 20 μm × 20 μm, to 10 μm × 10 μm demonstrated that Al sites detected using coarser spatial resolutions were always detected in the finer spatial

Table 1. Beam Spot[a] and Charge Collection Optimization for the Detection of Al Localizations

beam spot or pixel size (μm)	beam spot or pixel size (μm)	approximate analysis time (min)	charge (μC)	charge/ pixel (nC)	charge/ μm² (nC/μm²)	Al mdl/ pixel (mg/kg)	Al mass mdl/pixel (pg)	pixels with Al	% of Al pixels that register with Al pixels in the next larger pixel size	no. of Al localizations	Al mass detected (pg)	average Al tissue concentration (mg/kg)
50 × 50	2500	80	10.000	100	0.0400	118	2.9	1	NA[b]	1	3.0 ± 0.6	1.2 ± 0.2
50 × 50	2500	8	1.000	10	0.0040	402	11.1	0	NA	0	none	NA
50 × 50	2500	1	0.100	1	0.0004	1498	37.5	0	NA	0	none	NA
20 × 20	400	80	10.000	16	0.0400	309	1.24	2	50	2	5.7 ± 1.0	2.3 ± 0.4
20 × 20	400	8	1.250	2	0.0050	962	3.85	0	0	0	none	NA
20 × 20	400	1	0.625	1	0.0025	1428	5.71	0	0	0	none	NA
10 × 10	100	100	12.500	5	0.0500	529	0.52	5	60	4	10.3 ± 1.7	4.1 ± 0.7
10 × 10	100	20	2.500	1	0.0100	1376	1.38	5	60	4	9.8 ± 1.6	3.9 ± 0.7
10 × 10	100	2	1.250	0.5	0.0050	1827	1.83	4	50	4	9.2 ± 1.6	3.7 ± 0.6
5 × 5	25	160	20.000	2	0.0800	927	0.23	15	93	4	10.6 ± 1.8	4.2 ± 0.8
5 × 5	25	80	10.000	1	0.0400	1302	0.33	14	100	4	10.9 ± 1.8	4.4 ± 0.8
5 × 5	25	40	5.000	0.5	0.0200	1901	0.48	14	100	4	9.8 ± 1.6	3.9 ± 0.7
1.5 × 1.5	2.25	1232	22.18	0.2	0.0889	3027	0.07	65	91	4	11.1 ± 1.7	4.5 ± 0.9

[a] The beam current was ~2 nA for beam spots from 50 μm × 50 μm to 5 μm × 5 μm and 300 pA for beam spot 1.5 μm × 1.5 μm. [b] NA means not applicable.

resolution scans. The 10 μm × 10 μm pixel size was determined to be the most efficient beam spot size for identifying and quantifying Al localizations within the analyzed region using beam currents of 2−3 nA. Beam spot sizes of less than 10 μm × 10 μm did not increase the sensitivity or quantitative accuracy; however, the finer beam spot sizes did detect greater numbers of Al localizations, thus resulting in increased spatial resolution. Increased spatial resolution may be very important for some studies; however, this increase is achieved only with a substantial increase in data collection times. For example, imaging with a 5 μm × 5 μm beam spot with 1 nC per pixel charge collection would require 400% more instrument time than the 10 μm × 10 μm beam spot with 1 nC per pixel charge collection. This work demonstrates that a 10 μm × 10 μm beam spot size provides the best combination of Al quantitation (the most sensitive), localization, and decreased data collection time. For experiments that require maximum spatial resolution, the 10 μm × 10 μm beam spot size could first be used to scan the sample to identify and quantitate Al localizations. Following which, higher-spatial resolution scans utilizing finer beam spots could then be limited to only those areas demonstrated to contain Al localizations. The method is applicable for other metals and biological samples, although each may require its own specific PIXE setting.

To demonstrate the utility of this experimental protocol, we analyzed a limited number of olfactory and brain tissues obtained from F344 rats exposed to Al via nose-only exposure (Table 2). Significantly greater concentrations of Al were found in the olfactory tissue than in deeper brain tissue ($p > 0.05$), and a correlation was observed between Al concentration present in olfactory tissue and deeper brain tissues ($p > 0.1$). Given the limited number of animals and tissue samples analyzed, it is difficult to make definitive statements concerning olfactory transport of Al and possible subsequent transport to deeper brain regions; however, it does not support systemic transport and deposition and favors the hypothesis of direct transport via the olfactory epithelium to the bulb. The significant increase in the Al level in olfactory bulbs as compared to that in brain and the correlation between olfactory Al content and brain Al content warrant further studies.
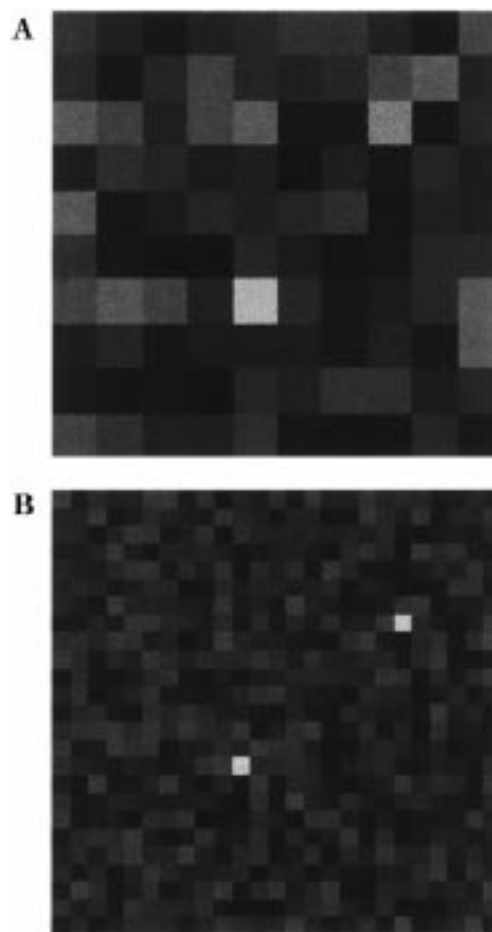

Figure 2. (A) Map of detected X-rays from the energy region from 1.4 to 1.6 keV of a 0.5 mm × 0.5 mm region scanned with a 50 μm beam spot using a 50 μm × 50 μm pixel size and a dose of 100 nC/pixel. The color scale is proportional to X-ray counts and ranges from black (minimum X-ray counts) through gray to white (maximum X-ray counts). This energy window includes X-rays from Al. Only one pixel (the white pixel toward the center of the image) has detectable amounts of Al. (B) Map of detected X-rays from the energy region from 1.4 to 1.6 keV of the same region depicted in panel A but scanned with a 20 μm beam spot using a 20 μm × 20 μm pixel size and a dose of 16 nC/pixel. In comparison with panel A, this image has two regions containing detectable amounts of Al (white pixels): the one previously detected in panel A and an additional pixel.

Table 2. Number of Al Localizations and Average Al Concentration[a]

tissue[b] sample	Al sites	average concentration (mg/kg)[c]
1A	8	3.0 ± 0.5
2A	7	3.8 ± 0.6
3A	13	7.0 ± 1.7
4A	7	2.1 ± 0.4
1B	2	0.7 ± 0.2
2B	1	0.5 ± 0.1
3B	3	1.0 ± 0.2
4B	2	0.6 ± 0.2

[a] All tissue samples were scanned over an area of 1 mm × 1.5 mm. [b] Samples 1A–4A are olfactory bulbs tissue sections, and samples 1B–4B are nonolfactory bulb tissue sections. [c] Average concentration of Al detected in the whole 1 mm × 1.5 mm scanned region determined using the same procedure used to produce Al concentrations in column 13 of Table 1.

References

(1) McMillan, D. E. (1997) Manganese: Are there Effects from Long-Term, Low Level Exposure? 15th International Neurotoxicology Conference, Little Rock, AR.

(2) McLaughlin, A. I., Kazantizis, G., King, E., Teare, D., Porter, R. J., and Owen, R. (1962) Pulmonary fibrosis and encephalopathy associated with the inhalation of Al dust. *Br. J. Ind. Med.* **19**, 253–261.

(3) Ardvidson, B. (1983) Epidemiological data from occupational exposures to metal dust. In *Neurobiology of the Trace Elements*, Chapter 2, pp 51–78, Humana Press, Clifton, NJ.

(4) Tanner, C. M. (1992) Occupational and environmental causes of Parkinsonism. *Occup. Med.* **7**, 503–513.

(5) Tanner, C. M., Ottman, R., Goldman, S. M., Ellenberg, J., Chan, P., Mayeux, R., and Langston, J. W. (1999) Parkinson disease in twins-an etiologic study. *JAMA, J. Am. Med. Assoc.* **281**, 341–346.

(6) Tomlinson, A. H., and Esiri, M. M. (1983) Immunohistological demonstration of spread virus via olfactory pathways in mice. *J. Neurol. Sci.* **60**, 473–484.

(7) Shipley, M. T. (1985) Transport of molecules from nose to brain: transneuronal anterograde and retrograde labeling in the rat olfactory system by wheat germ agglutinin-horseradish peroxidase applied to the nasal epithelium. *Brain Res. Bull.* **15**, 129–142.

(8) Baker, H., and Spencer, R. F. (1986) Transneuronal transport of peroxidase-conjugated wheat germ agglutinin (WGA-HRP) from the olfactory epithelium to the brain of the adult rat. *Exp. Brain Res.* **63**, 461–473.

(9) McLean, J. H., Shipley, M. T., and Bernstein, D. I. (1989) Golgi-like, transneuronal retrograde labelling with CNS injections of herpes simplex virus type-1. *Brain Res. Bull.* **22**, 867–881.

(10) Muller-Klieser, W., and Walenta, S. (1993) Geographical mapping of metabolites in biological tissue with quantitative bioluminescence and single photon imaging. *Histochem. J.* **25**, 407–420.

(11) Linton, R. W., and Goldsmith, J. G. (1992) The role of secondary ion mass spectrometry (SIMS) in biological microanalysis: technique comparisons and prospects. *Biol. Cell* **74**, 147–160.

(12) Cookson, J. A., Ferguson, A. T. G., and Pilling, F. D. (1972) Proton microbeams, their production and use. *J. Radioanal. Chem.* **12**, 39–52.

(13) Johansson, S. A. E., and Campbell, J. L. (1988) *PIXE-A Novel Technique for Elemental Analysis*, Wiley & Sons, Chichester, U.K.

(14) Raabe, O. G., Bennick, J. E., Light, M. E., Hobbs, C. H., Thomas, R. L., and Tillery, M. I. (1973) An improved apparatus for acute inhalation exposure of rodents to radioactive aerosols. *Toxicol. Appl. Pharmacol.* **26**, 264–273.

(15) Cheng, Y. S., Barr, E. B., and Yeh, H. C. (1989) A venturi disperser as a dry powder generator for inhalation studies. *Inhal. Toxicol.* **1**, 365–371.

(16) Roberts, M. L., Bench, G. S., Heikkinen, D. W., Morse, D. H., Bach, P. H., and Pontau, A. E. (1995) The new nuclear microprobe at Livermore. *Nucl. Instr. Methods Phys. Res., Sect. B* **104**, 13–18.

(17) Morse, D. H. (1994) A data-acquisition system for scanning microbeam analysis. *Nucl. Instr. Methods Phys. Res., Sect. B* **85**, 693–698.

(18) Meanhaut, W. (1990) Multielement analysis of biological materials by particle-induced X-ray emission (PIXE). *Scanning Microsc.* **4**, 43–62.

(19) Antolak, A. J., Bench, G. S., and Morse, D. H. (1994) IMAP: A complete ion microanalysis package for the nuclear microprobe. *Nucl. Instr. Methods* **B85**, 597–601.

(20) Lefevre, H. W., Schofield, R. M. S., Overley, J. C., and McDonald, J. C. (1987) Scanning transmission ion microscopy as it complements particle induced X-ray emission microscopy. *Scanning Microscopy* **1**, 879–889.

(21) Campbell, J. L., Maenhaut, W., Bombelka, E., Clayton, E., Malmqvist, K., Maxwell, J. A., Pallon, J., and Vandenhaute, J. (1986) An intercomparison of spectral data processing techniques in PIXE. *Nucl. Instr. Methods Phys. Res., Sect. B* **14**, 204–220.

(22) Antolak, A. J., and Bench, G. S. (1994) PIXEF: The Livermore PIXE spectrum analysis package. *Nucl. Instr. Methods Phys. Res., Sect. B* **90**, 596–601.

TX9900268